Effect of EVA as Compatibilizer on the Mechanical Properties, Permeability Characteristics, Lamellae Orientation, and Long Period of Blown Films of HDPE/Clay Nanocomposites

Juliano Marini,[1] Márcia Cristina Branciforti,[1] Rosa Maria Vercelino Alves,[2] Rosario Elida Suman Bretas[1]

[1]*Department of Materials Engineering, Universidade Federal de São Carlos, São Carlos 13565-905, SP, Brazil*
[2]*Packaging Technology Center (CETEA), Instituto de Tecnologia de Alimentos, Campinas 13070-178, Brazil*

Received 30 October 2009; accepted 24 February 2010
DOI 10.1002/app.32356
Published online 14 July 2010 in Wiley InterScience (www.interscience.wiley.com).

ABSTRACT: Two ethylene-vinyl acetate (EVA) resins with 19% (EVA19) and 28% (EVA28) of vinyl groups were used as compatibilizers for nanocomposites of high-density polyethylene (HDPE) and nanoclays. Two nanoclays were also used, one with a nonpolar surfactant (C15A) and another with a polar surfactant (C30B). The HDPE/EVA19/C15A formed an intercalated structure, while the HDPE/EVA28/C30B had surfactant loss. Blown films of these compositions were produced. A two-phase morphology made of HDPE and EVA/nanoclay particles was observed, which was responsible for the increase in water vapor and oxygen permeability rates of the films. The elastic modulus E along the transverse direction of the films was higher than along the machine direction due to preserved orientation given by the spiral die; the lamellae orientation was measured by small-angle X-rays diffraction. The highest E was observed in the HDPE/EVA19/C15A film due to stronger interactions. The long period of the HDPE lamellas was not affected by the presence of the EVA and nanoclay. A model was proposed to explain the improvement in elastic modulus due to the processing conditions and components' interactions. © 2010 Wiley Periodicals, Inc. J Appl Polym Sci 118: 3340–3350, 2010

Key words: nanocomposites; blown films; compatibility; mechanical properties; SAXS

INTRODUCTION

The film blowing process is one of the most important techniques to produce flexible packing from polyolefins like low density polyethylene (LDPE), high-density polyethylene (HDPE), and linear low density polyethylene (LLDPE) among others. The final properties of the blown films depend on morphology which is influenced by the processing conditions. However, sometimes the control of the processing conditions is not enough to optimize the morphology that would give the best mechanical and transport properties and thus, extrusion of blown films with multiple layers and reinforcing fillers are used to improve those properties.

In recent years, the use of nanoparticles as reinforcing fillers in polymers has considerably grown, because the addition of a very small amount of these particles to the polymer can increase substantially its mechanical and transport properties, especially in polyolefins.[1–3] The improvement, in the case of lamellar nanoclays, is accomplished when the clay is exfoliated or intercalated and well distributed through the polymer matrix.[4,5] Clays can be efficiently exfoliated in polar polymers when the correct processing conditions are used[6,7]; however, when the polymer is a polyolefin, usually the attainment of exfoliated structures is more complicated due to the polyolefin's hydrophobic character and to the lack of interactions with the hydrophilic surface of the clay. Therefore, treatment of the clay's galleries must be done; it is usually made with organic modifiers (surfactants), which can have polar or nonpolar groups. Even so, in some cases, when the final interactions between the polyolefin and the organoclay are weak or scarce, a compatibilizer needs to be used. This compatibilizer usually is a copolymer with a nonpolar backbone and a grafted polar monomer, for example, like the standard polyethylene or polypropylene grafted with maleic anhydride (PEgMA or PPgMA, respectively) or polyethylene grafted with acrylic acid (PEgAA).[8–11] Other copolymer, ethylene–vinyl acetate (EVA) can also be used as compatibilizer. EVA is a random copolymer, in which the amount of vinyl acetate (VA) groups can

Correspondence to: R. E. S. Bretas (bretas@ufscar.br).
Contract grant sponsors: CAPES and FAPESP.

vary, changing its polarity; the presence of these polar groups makes this copolymer more compatible with organic modified clays than polyethylene.[12–16] Studies[17–19] have shown that the addition of EVA in nanocomposites of LDPE and HDPE with organoclays improved the polymer intercalation into the clay's platelets; however, the efficiency of the compatibilization was dependent of the EVA amount and the VA content.

The processing parameters of the film blowing process have also influence on the final properties of the films of nanocomposites. Recent work from our lab[1] showed that films of intercalated nanocomposites of HDPE/PEgMA/clay that were produced with high elongation rate during the film blowing process had higher elastic modulus and lower water vapor permeability rates than films blown at a low elongation rate, due to the clay and macromolecules orientation during the blowing. The relationship between processing conditions, morphology, and properties (mechanical, thermal, permeability) in polyethylene nanocomposites have been studied[2,20,21] and in general, it is observed that the improvement on the nanocomposites properties is dependent of the intercalation/exfoliation level, orientation of clay platelets and the degree of their dispersion.

From these studies, it can be concluded that both, EVA and PEgMA can be used as compatibility agents between polyethylenes and nanoclays. However, EVA not being a grafted or block copolymer, probably will have a lower efficiency as a compatibility agent than the PEgMA; on the other hand, EVA has a much lower cost than PEgMA. Thus, the objective of this work was to study the effect of the addition of EVA as a compatibility agent on the mechanical and barrier properties, long period, and lamellae orientation of blown films of HDPE/clay nanocomposites.

EXPERIMENTAL

Materials

The same resin used in our earlier work[1] was chosen as polymer matrix; it was a HDPE (film blowing grade) of weight average molecular weight (M_w) of 420,907 g/mol and molecular weight distribution of 20.89; its other properties are listed in Table I. The supplier added an antioxidant to avoid extensive thermal degradation. To study the influence of the VA content on compatibilization, two types of EVA resins (EVA19 and EVA28) were used; according to the supplier, the EVA19 had 19% of VA groups while the EVA28 had 28% of VA groups. The properties of the EVA resins are also listed in Table I.

To study the influence of the polarity of the nanoclay's surfactants on the exfoliation/intercalation levels, two types of montmorillonite clays were also used; one was treated with a nonpolar surfactant (C15A) and the other one with a polar surfactant (C30B). The properties of both nanoclays are also given in Table I while the chemical structures of the surfactants (quaternary alkyl ammonium salts) are shown in Figure 1.

Thermal stability of the nanoclays

The thermal stability of the nanoclays was studied by high resolution thermogravimetrical analysis (TGA) using an equipment from TA Instruments, model HiRes TGA 2950, at a heating rate of 20°C/min, from room temperature up to 500°C, under N_2 flux.

Extrusion of the nanocomposites

The nanocomposites were produced by corotational twin-screw extrusion, using an extruder from Werner Pfleider, model ZSK 30, with diameter of 30

TABLE I
Properties of the HDPE, EVA Resins, and Nanoclays

	HDPE	EVA 19	EVA 28	C15A	C30B
Trade name	HF0150	Evateno 8019-PE	Elvax 250	Cloisite® 15A	Cloisite® 30B
Supplier	Braskem	Braskem	Dupont	Southern Clay	Southern Clay
Density (g/cm^3)	0.948[a]	0.940[a]	0.921[a]	0.30[b]	0.36[b]
MFI (g/10min)	10.0[c]	8.0[d]	25.0[d]	–	–
%VA[e]	–	19	28	–	–
Melting Point (°C)[f]	128	57/86	50/72	–	–
Gallery Distance (nm)[e]	–	–	–	3.15	1.85
Surfactant concentration (meq/100g clay)[e]	–	–	–	125	90

[a] ASTM D-1505.
[b] According to the supplier.
[c] ASTM D-1238 (190°C/21.6 Kg).
[d] ASTM D-1238 (190°C/2.16 Kg).
[e] According to the supplier.
[f] As measured by differential scanning calorimetry, in a TA instruments, model QS100, 10°C/min.

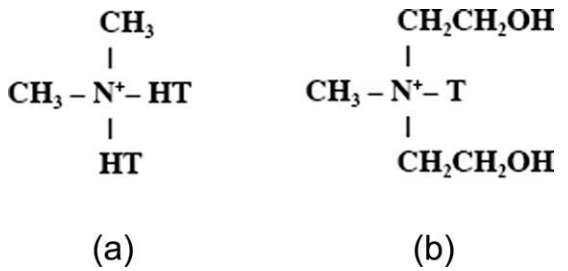

Figure 1 Chemical structures of the nanoclay's surfactants: (a) C15A; (b) C30B; HT = alkyl group with ~ 65% C_{18}, ~ 30% C_{16}, and ~ 5% C_{14}.[22]

mm and length of 1070 mm; the screws' profile was similar to the one used in our earlier work,[1] highly dispersive with transport, kneading, and turbine elements, as shown in Figure 2.

The nanocomposites of HDPE/EVA/nanoclay were obtained in two steps: (1) extrusion of an EVA/nanoclay masterbatch and (2) dilution of the masterbatch in HDPE, also by extrusion. The masterbatches had final concentration of EVA/nanoclay of 75/25 wt % and were extruded at a flow rate of 2.5 kg/h, velocity of 120 rpm (which resulted in an average residence time of approximately 100 s) and temperatures between 110 and 140°C. The nanocomposites had a final concentration of HDPE/EVA/nanoclay of 80/15/5 wt % and were extruded at the same flow rate and velocity as the masterbatches, but at temperatures between 215 and 225°C.

Films blowing

Blown films of HDPE and HDPE/EVA/clay nanocomposites were produced using a film blowing extruder from Miotto. The screw had a diameter D = 25 mm, length L = 750 mm, and angle $\theta = 17.7°$. The spiral die had an external diameter D_e = 80 mm, internal diameter D_i = 78.4 mm, and extended length L_m = 640 mm. All the films were blown at the same conditions: screw rotation N = 80 rpm and nip rolls velocity V_p = 1 m/min. The extrusion temperatures were set between 200 and 225°C. The take-up ratio (TUR = V_p/V_e, where V_e is the extrusion rate) was 4, while the blow up ratio (BUR = R_f/R_d, where R_f is the final film radius and R_d is the die radius) was 1. V_e was calculated from the mass rate $Q = \rho \cdot V_e/A_d$, where ρ is the polymer density and A_d the transversal area of the spiral die. Q was the mass of blown film collected after 1 min of blowing. The blown films had an average thickness of 200 ± 15 μm and average diameter of 80 ± 4 mm.

Characterization of the nanocomposites and the blown films

Rheological characterization

The complex viscosity η^* (ω) of the nanocomposites was measured using a controlled stress rheometer from Rheometric Scientific, model SR-5000, at 225°C, with geometry of parallel plates, plates' diameter of 25 mm and gap between the plates of 1 mm, under nitrogen atmosphere. The measurements were done between 0.01 and 100 rad/s, in the linear viscoelastic region.

Wide-angle X-ray diffraction

To analyze the exfoliation/intercalation level of the nanocomposites, a diffractometer Rigaku Multiflex, with CuK_α radiation (λ = 1.54058 Å), operating at 30 kV and 10 mA was used; the samples were scanned between 0.8 and 10° at a rate of 1°/min.

Transmission electron microscopy

To analyze the dispersion and distribution levels of the clay in the nanocomposites, samples were prepared by cryo-ultra microtomy at −55°C using a microtome from Leica, model Reichert Ultracut FC4;

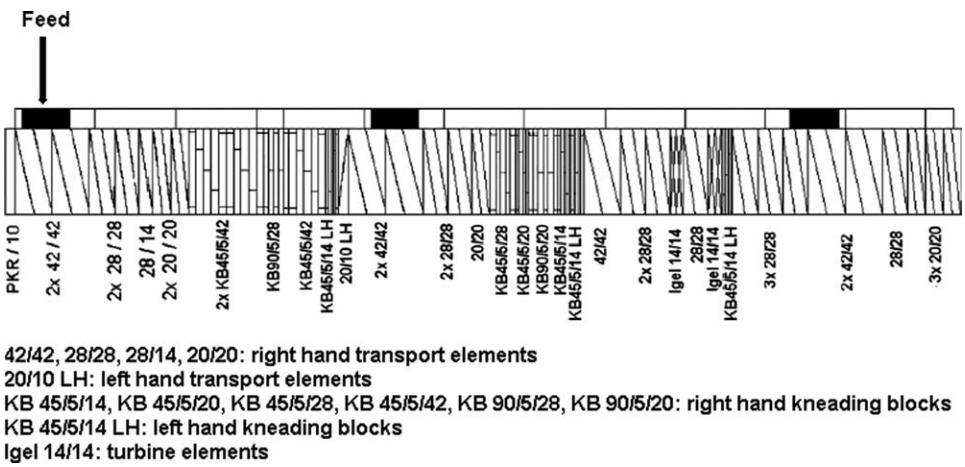

Figure 2 Profile of the twin-screw extruder used in this work.[1]

the microtomed films were analyzed in a transmission electron microscope from Phillips, model CM 120, operating at 120KV. To distinguish the HDPE from the EVA, the samples were stained with RuO_4, during 2 h at 60°C.[23,24]

Atomic force microscopy

The surface roughness of the blown films was measured by atomic force microscopy (AFM) using a microscope from Veeco Digital Instruments, model MMA FM-2, in the tapping mode, with an Si probe. The scanning was made on 10 μm x 10 μm areas. The average surface roughness (RMS) was calculated using the Nanoscope IIIa software from Veeco Digital Instruments.

Optical properties

The total haze of the films was measured in a Haze Gard Plus equipment from BYK-Gardner, following ASTM D-1003 standard procedure. Five samples of each film were analyzed.

Mechanical properties

The tensile properties of the films in the machine direction (MD) and transverse direction (TD) to the MD were measured following ASTM D-882 standard procedure in an Instron Tensile Testing machine, model 5569, at room temperature. At least five measurements of each sample were made. Strips of 25 mm width and 190 mm length were obtained using film cutting equipment from Frank Prufgerate GMBH.

Small-angle X-ray scattering

To estimate the lamellae orientation of the films, small-angle X-ray scattering (SAXS) measurements were done at the D11A-SAXS line of the Brazilian Synchrotron Light Laboratory (LNLS). The beam energy was tuned to 8049.9 eV, with $\lambda = 1.7556$ Å. The incident beam was collimated by a 3 × 1.6 mm diffraction slit coupled with a 0.5 mm slit located just before the detector. The beam was positioned perpendicular to MD and TD. The SAXS scattering data was collected in the form of a 2-D image. A radial average was then performed on the 2-D scattering pattern, which was a quantitative measure of the intensity of X-ray scattering. From the radial average plots, the Hermann's orientation factors (f) following Prasad et al. procedure[25] were obtained using eq. (1):

$$f = \frac{(3 \cdot \cos^2 \phi) - 1}{2} \quad (1)$$

in which ϕ is the angle between the reference axis and the macromolecule chain axis (in HDPE, this latter axis is the **c**-axis of the orthorhombic unit cell). The reference axis was MD. It is worthwhile to point out that when $f = 1$, complete lamellae orientation along MD will occur; when $f = -0.5$ perpendicular to MD orientation will occur and when $f = 0$, random orientation (isotropic sample) will occur.

The long period L (distance between the middle of two polymeric lamellas), which defines the periodicity of lamellar stacking was also measured. The experimental SAXS curves were corrected (elimination of additional scattering caused by optical elements in the X-rays path and corrections due to possible inconsistencies in the electronic density within each phase caused by temperature, using the Bonart method); thus, standard light intensity (I_{cor}) versus scattering vector (q) curves were obtained. The first peak of these curves represented the scattering produced by the crystalline lamellas with thickness L_c that were periodically separated by an amorphous phase of thickness L_a, corresponding to a two-phase model ($L = L_c + L_a$). Therefore, L was calculated from eq. (2):

$$L = \frac{2\pi}{q^*} \quad (2)$$

in which q^* is the maximum peak of the $I_{cor}(q).(q)^2$ versus q curve.

Permeability rates

The water vapor permeability rate (WVPR) of the films was measured in a Permatran equipment with infrared sensor, Model W 3/31, from Mocon, following ASTM F-1249-01 standard procedure at 38ºC and 100% humidity. The water vapor permeability coefficient (WVPC) was calculated from eq. (3):

$$\mathrm{WVPC} = \frac{\mathrm{WVPR} \times e}{p_s \times \mathrm{RU}_1} \quad (3)$$

in which e is the average thickness of the film, p_s is the vapor saturation pressure at the test temperature (49.692 mmHg at 38°C), and RU_1 is the chamber relative humidity (100%).

The oxygen permeability rate (OPR) was measured by the coulometric method following ASTM D-3985 standard procedure in an Oxtran equipment, model ST, from Mocon, operating with pure and dry oxygen at 23°C. The oxygen permeability coefficient (OPC) was calculated from eq. (4):

$$\mathrm{OPC} = \frac{\mathrm{OPR} \times e}{p} \quad (4)$$

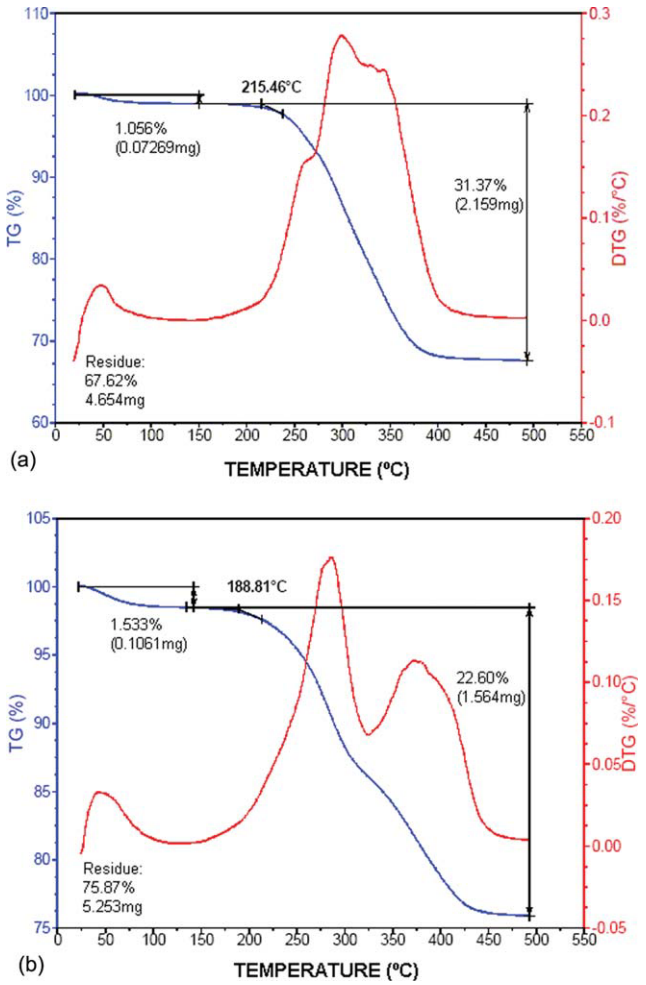

Figure 3 Thermogravimetric analyses of the nanoclays: (a) C15A; (b) C30B. [Color figure can be viewed in the online issue, which is available at www.interscience.wiley.com.]

in which p is the oxygen partial pressure in the chamber (1 atm). For these tests the films thickness was measured with a micrometer of planar nib, model 732, from STARRETT, with resolution of 0.001 mm.

RESULTS AND DISCUSSION

Characterization of the materials

The TGA of both nanoclays is shown in Figure 3; in both samples, two peaks in the derivative of the TG (DTG) curves are observed. The first peak is due to water loss (1.056% in the C15A and 1.533% in the C30B). The second peak is attributed to the loss of surfactant and other organic impurities.[26] The surfactant loss begun at 215°C in the C15A nanoclay, whereas in the C30B nanoclay it begun at 188°C. As described before, the masterbatches were extruded between 110 and 140°C; therefore, it was assumed that during the masterbatches' extrusion no surfactant loss occurred. The nanocomposites were extruded between 215 and 225°C, with a residence time of 100 s. Under these last conditions, however, surfactant loss could have occurred.

Characterization of the extruded samples

The complex viscosities of the materials are shown in Figure 4; it can be observed that none of the materials had a Newtonian behavior at low shear rates; instead, a pseudoplastic behavior is observed at all shear rates. It is also observed that both nanocomposites had lower viscosities than the pure HDPE, that is, the EVA and nanoclay plasticized the HDPE. Thus, it is expected that during the film blowing process, lower mechanical energies will be spent during the extrusion of the nanocomposites than during the extrusion of the HDPE. The viscosity of the EVA28 at 225°C was extremely low, out of the rheometer's sensitivity range and it was not measured.

Figure 5 shows the diffractograms of both systems, while Table II shows the distance between clay lamellas, calculated from these diffractograms. The results indicated that an intercalated structure in the nanocomposite HDPE/EVA19/C15A was predominant; however, in the nanocomposite HDPE/EVA28/C30B, a decrease in the galleries' distance was observed, which could be due to surfactant loss. In a previous work in our labs,[27] however, the EVA28/C30B nanocomposite showed an exfoliated structure after mixing in a torque rheometer; thus, probably the high deformation rates and temperatures of the twin-screw extruder accelerated the degradation of the C30B surfactant.

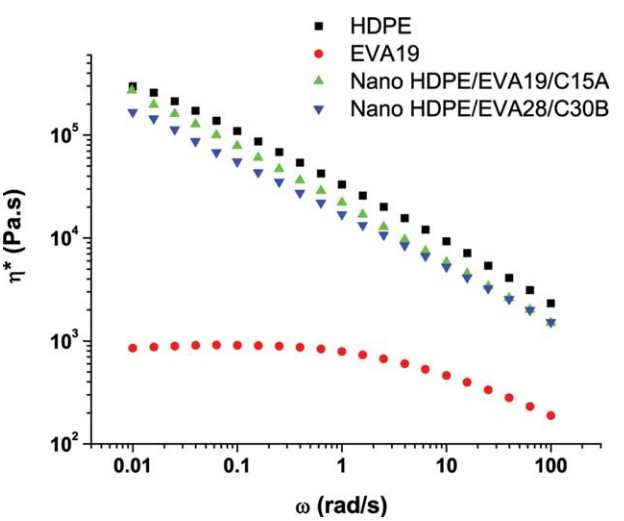

Figure 4 Complex viscosity η* of the polymers, at 225°C. [Color figure can be viewed in the online issue, which is available at www.interscience.wiley.com.]

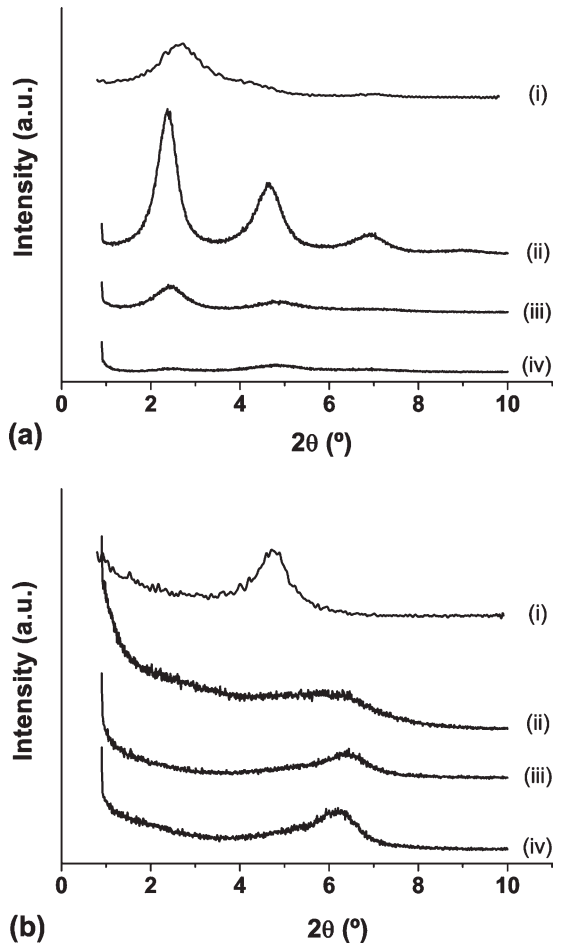

Figure 5 WAXD curves of the (a) HDPE/EVA19/C15A system – (i) C15A, (ii) Masterbatch EVA19/C15A, (iii) Nano HDPE/EVA19/C15A, (iv) Film HDPE/EVA19/C15A - and (b) HDPE/EVA28/C30B system – (i) C30B, (ii) Masterbatch EVA28/C30B, (iii) Nano HDPE/EVA28/C30B, (iv) Film HDPE/EVA28/C30B.

Figure 6(a) shows a Transmission electron microscopy (TEM) micrograph of the extruded HDPE/EVA19/C15A nanocomposite; the dark areas represent the EVA phase after staining with RuO_4. The C15A clay is predominantly inside the EVA phase. Figure 6(b) shows an enlargement of an EVA particle; clay's lamellas are observed inside the EVA phase and at the interface HDPE/EVA. To analyze the clay's dispersion level, samples without RuO_4 staining were also analyzed and are shown in Figure 6(c); a good distribution of the clay's tactoids thru the HDPE/EVA matrix is observed, confirming the rheological results.

Figure 7(a) shows a micrograph of the extruded HDPE/EVA28/C30B system; again, clay's tactoids inside the EVA phase are observed.

Films blowing and characterization

During the film blowing process the torque developed during the extrusion of the HDPE film was 90% of the maximum torque, while the torques developed during the extrusion of the HDPE/EVA19/C15A and HDPE/EVA28/C30B nanocomposites were 60 and 50% of the maximum torque, respectively, confirming the decrease in mechanical energy predicted by the results of complex viscosity.

Wide-angle X-ray diffraction (WAXD) diffractograms of the blown films are also shown in Figure 5. The clay's intercalated structure of the HDPE/EVA19/C15A nanocomposite and the clay's structure of the HDPE/EVA28/C30B system were preserved after film blowing. Figures 6(d) and 7(b) show TEM micrographs of the blown films of both systems, respectively; both systems had highly oriented EVA/clay particles along MD.

Figure 8 shows AFM micrographs of the blown films while Table III shows the average roughness. A decrease of 55 and 32% in the average roughness of the blown films of the C15A and C30B nanocomposites, respectively, compared with the pure HDPE film was observed. The decrease in surface roughness can be correlated to the decrease in surface haze, and consequently to the decrease in total haze.[28–31] The total haze of each film is shown in Table III. The total haze has two components: internal (bulk) and surface haze. The internal haze is dependent mostly on the crystals sizes and morphologies, whereas the surface haze is mostly dependent on the surface roughness. In the case of blown films, generally, the surface haze is the major component; Wilkes and coworkers[28,31] and Bretas and coworkers[29,30] have found, for example, that the surface haze in blown films usually represents 60–80% of the total haze. Thus, it can be observed that the total haze of the nanocomposites' films decreased as their surface roughness decreased.

The tensile stress–strain curves of the blown films are shown in Figure 9. The calculated values of the tensile elastic modulus E, yield stress σ_y, ultimate stress σ_b, ultimate strain ε_b, and toughness, along MD and TD of the blown films are shown in Table IV and V, respectively.

Along MD, it is observed that the addition of the EVA19 and the C15A nanoclay to the HDPE did not

TABLE II
Distance Between Clay Lamellas Calculated from the Diffractograms

Material	2θ (°)	d_{001} (nm)
C15A	2.7	3.28
Masterbatch EVA19/C15A	2.4	3.70
Nano HDPE /EVA19/C15A	2.4	3.70
Film HDPE /EVA19/C15A	2.4	3.70
C30B	4.7	1.88
Masterbatch EVA28/C30B	6.2	1.43
Nano HDPE/EVA28/C30B	6.2	1.43
Film HDPE/EVA28/C30B	6.4	1.38

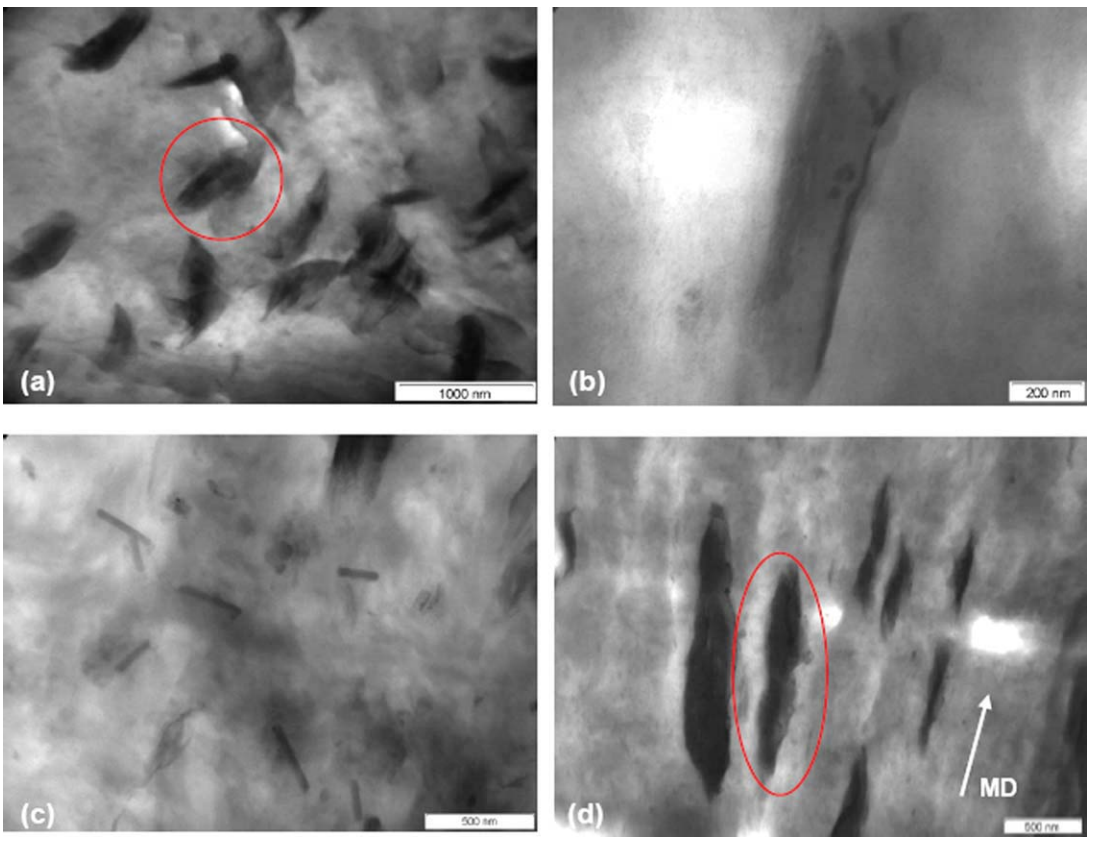

Figure 6 TEM micrographs of the HDPE/EVA19/C15A nanocomposite. (a) Extruded nancomposite (stained); (b) Enlargment of an EVA particle from the extruded nanocomposite (stained); (c) Extruded nanocomposite (not stained); (d) Blown film of the nanocomposite (stained). The circles highlight the EVA/nanoclays particles. [Color figure can be viewed in the online issue, which is available at www.interscience.wiley.com.]

change the elastic modulus of the blown films. However, the addition of the EVA28 and the C30B nanoclay to the HDPE decreased this modulus. The yield stress of both films of nanocomposites decreased, while the ultimate stresses and strains were not affected by the presence of the EVA and nanoclay. The toughness of both films of nanocomposites along MD also decreased. Along TD, the addition of the EVA19 and the C15A clay to the HDPE slightly increased the elastic modulus of the blown films, while the addition of the EVA28 and the C30B clay decreased this modulus. The yield stress of the HDPE/EVA19/C15A blown film was higher than of the pure HDPE film, whereas the HDPE/EVA28/

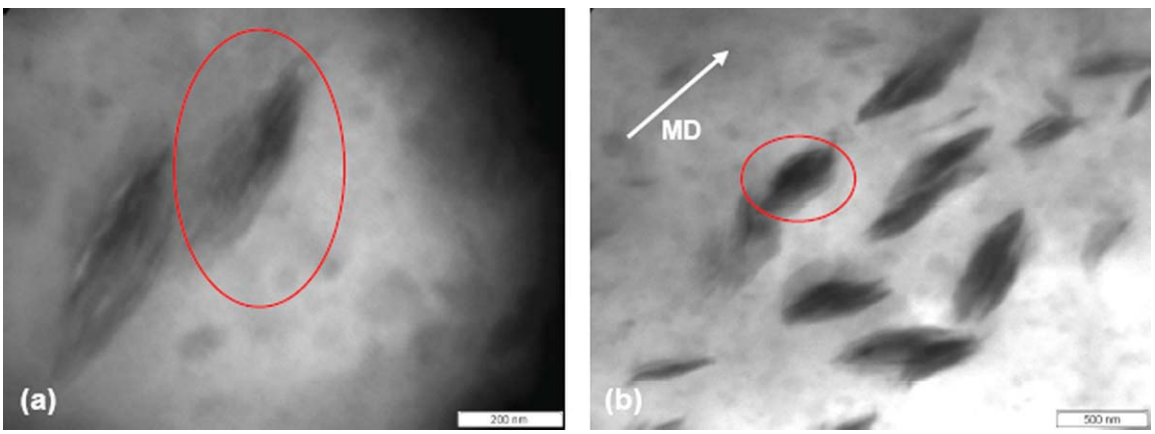

Figure 7 TEM micrographs of the HDPE/EVA28/C30B nanocomposite. (a) Extruded nanocomposite (stained); (b) Blown film of the nanocomposite (stained). The circles highlight the EVA/nanoclays particles. [Color figure can be viewed in the online issue, which is available at www.interscience.wiley.com.]

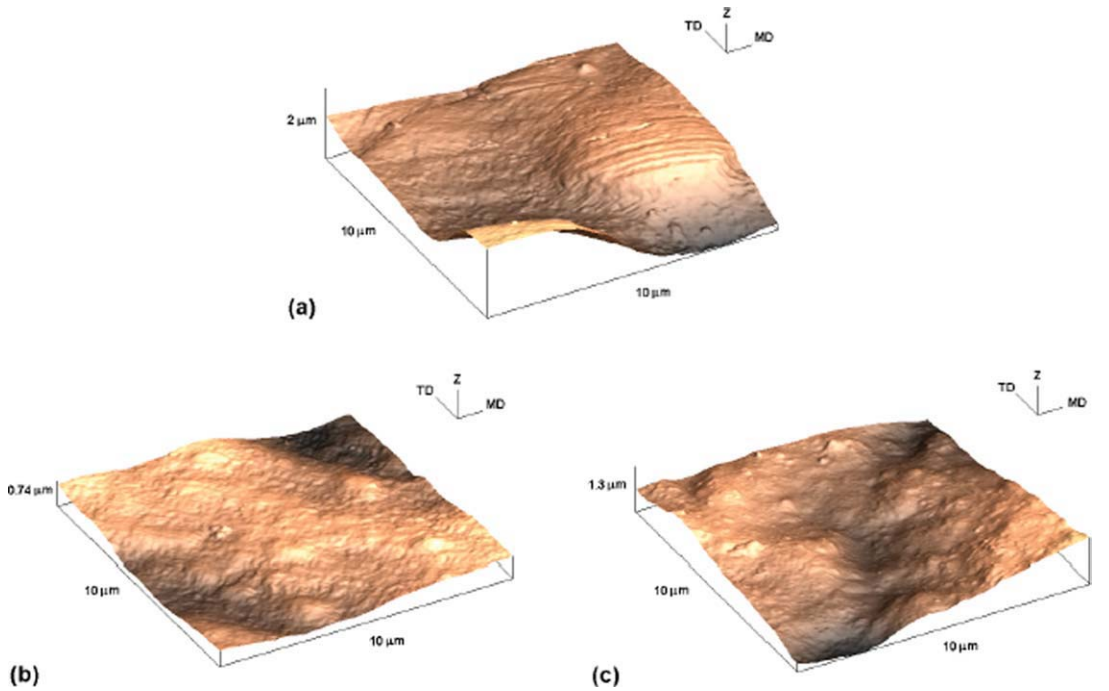

Figure 8 AFM micrographs of blown films: (a) HDPE; (b) HDPE/EVA19/C15A nanocomposite; (c) HDPE/EVA28/C30B nanocomposite. [Color figure can be viewed in the online issue, which is available at www.interscience.wiley.com.]

C30B had fragile fracture. The ultimate stresses and strains of the HDPE/EVA19/C15A film were similar to the HDPE film; however, the HDPE/EVA28/C30B film had worse ultimate properties than the HDPE. The toughness of the HDPE and HDPE/EVA19/C15A films were similar.

The better results obtained with the HDPE/EVA19/C15A nanocomposite than with the HDPE/EVA28/C30B nanocomposite can be credited to the stronger interactions between the HDPE, the EVA19 and the C15A nanoclay. The EVA19 was more compatible with the HDPE than the EVA28 due to its lower amount of VA groups[32,33]; on the other hand, the C15A nanoclay interacted more with the HDPE than the C30B nanoclay due to the nonpolarity of its surfactant.

Jordan et al.,[34] pointed out in their review of mechanical properties of nanocomposites, that the elastic modulus is more dependent on the nanofiller's

TABLE III
Average Surface Roughness (RMS), Total Haze, Long Period (*L*) and Hermann's Orientation factor (*f*) of the Blown films

Blown Film	RMS (nm)	Total Haze (%)	*L* (nm)	*f*
HDPE	353 ± 3	94.6 ± 1.1	30.28	−0.27
HDPE/EVA19/C15A	161 ± 6	90.9 ± 0.2	30.19	−0.35
HDPE/EVA28/C30B	241 ± 7	92.3 ± 0.1	30.18	−0.28

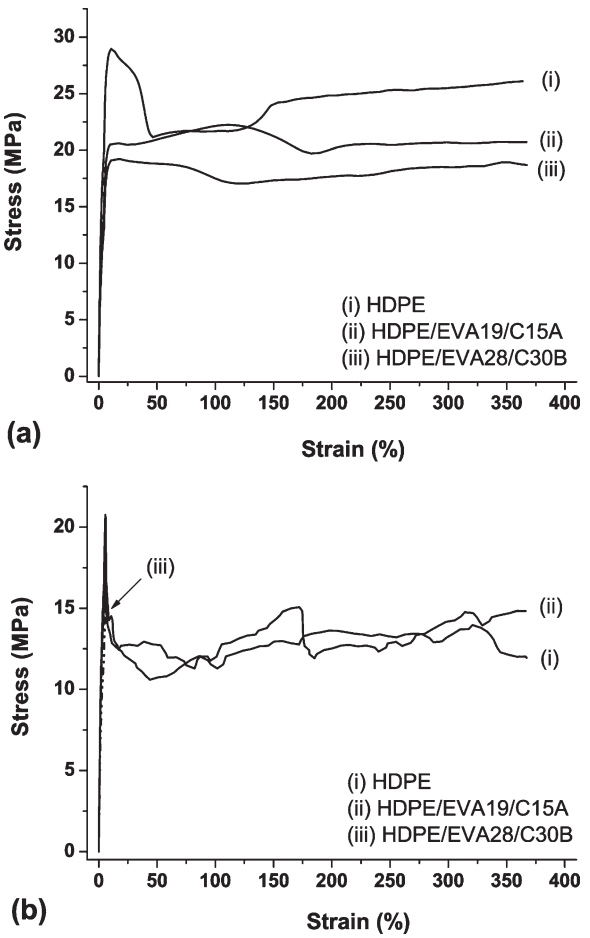

Figure 9 Tensile stress–strain curves of the blown films: (a) along MD; (b) along TD.

TABLE IV
Tensile Mechanical Properties Along MD of the Blown Films

Blown Film	E (MPa)	σ_y (MPa)	σ_b (MPa)	ε_b (%)	Toughness (GPa)
HDPE	776.4 ± 33.5	28.9 ± 0.8	No break[a]	No break[a]	(8.82 ± 0.61) x 10^2
HDPE/EVA19/C15A	778.2 ± 37.5	20.5 ± 1.0	No break[a]	No break[a]	(7.60 ± 0.42) x 10^2
HDPE/EVA28/C30B	641.3 ± 38.3	19.2 ± 0.8	No break[a]	No break[a]	(6.61 ± 0.29) x 10^2

[a] up to 360% strain

TABLE V
Tensile Mechanical Properties Along the TD of the Blown Films

Blown Film	E (MPa)	σ_y (MPa)	σ_b (MPa)	ε_b (%)	Toughness (GPa)
HDPE	843.4 ± 33.0	14.5 ± 0.6	No break[a]	No break[a]	(4.73 ± 0.25) x 10^2
HDPE/EVA19/C15A	847.4 ± 32.3	18.1 ± 1.1	No break[a]	No break[a]	(4.77 ± 0.30) x 10^2
HDPE/EVA28/C30B	647.3 ± 21.9	No flow[b]	14.9 ± 0.4	5.8 ± 0.8	6.47 ± 0.41

[a] Up to 360% strain.
[b] Fragile fracture.

characteristics (rigidity, particle size, and filler concentration) than on the interactions between the polymer and the nanofiller. However, the yield and ultimate properties are directly proportional to these interactions; when these latter mechanical properties are enhanced, strong interactions between the polymer matrix and the filler can be expected.

The elastic modulus along TD of all the blown films was also higher than the elastic modulus along MD. Because the TUR = 4 and BUR = 1, a different behavior was expected. To understand the mechanical behavior of the blown films of nanocomposites, the polymeric lamellae orientation and structural periodicity (long period) of the films were evaluated by SAXS. The 2-D SAXS patterns of the blown films are shown in Figure 10, while L and f values are shown in Table III.

The lamellar long period was found to be independent of the addition of EVA and nanoclay; that is, both materials did not alter the HDPE lamellar thickness and did not enter into its amorphous phase, as confirmed by other works.[21] This behavior can be attributed to the very low crystallinity of EVA,[35] to the low amount of EVA present in the nanocomposite and to the poor interactions between HDPE and EVA. Thus, it can be concluded that the measured f values correspond only to the HDPE lamellae orientation. As it is observed from Table III, the HDPE lamellas were preferentially oriented along TD, confirming the mechanical properties results. Because the HDPE had a high viscosity and elasticity, probably the imposed TUR was not high enough to align the HDPE macromolecules along MD and they preserved the orientation given by the extruder's spiral die. The EVA/nanoclays discrete particles, however, were aligned along MD; however, because the EVA19/C15A had stronger interactions with the HDPE than the EVA28/C30B discrete particles, the net result was an increase in the elastic modulus along TD due to the impediment of the HDPE lamellas to orient along MD given by the EVA19/C15A particles. A scheme to explain this behavior is shown in Figure 11. In this scheme, from our TEM and SAXS results, L ~ 30 nm, the length of a nanoclay's lamellas is approximately 200 nm and the EVA/clay discrete particles have length of approximately 1000 nm.

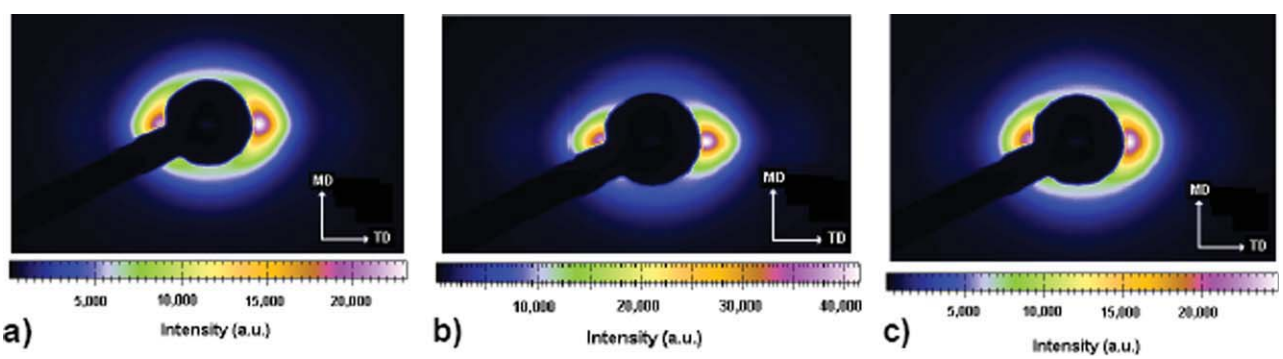

Figure 10 2-D SAXS patterns of blown films: (a) HDPE; (b) HDPE/EVA19/C15A nanocomposite; (c) HDPE/EVA28/C30B nanocomposite. [Color figure can be viewed in the online issue, which is available at www.interscience.wiley.com.]

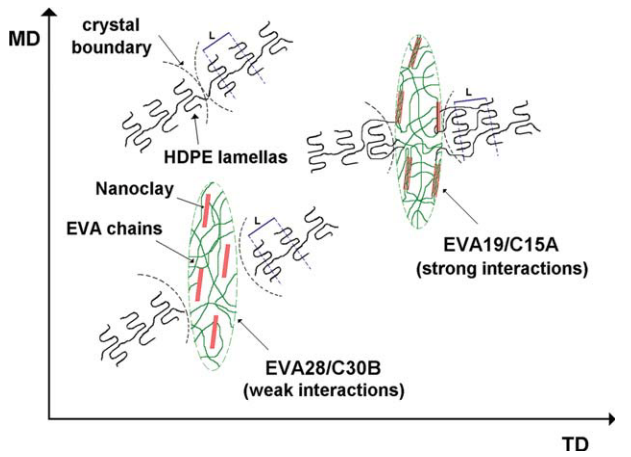

Figure 11 Scheme of the HDPE lamellae organization in the pure HDPE and nanocomposites films (L ~ 30 nm, length of a nanoclay's lamellas ~ 200 nm and length of EVA/clay discrete particles ~ 1000nm). [Color figure can be viewed in the online issue, which is available at www.interscience.wiley.com.]

Thus, it is concluded that the better mechanical properties of the HDPE/EVA19/C15A film along TD were due to a higher HDPE lamellae orientation along TD and to a better interaction between the HDPE, the EVA19 and the C15A nanoclay.

Table VI shows the results of the permeability rates of both systems. The van der Waals volumes of oxygen and water are similar[3,36]; however, the transport mechanisms of both penetrants in a flexible polymer are different, mainly because of their different polarity (which allows the formation of water clusters, for example). Regarding the WVPR, it can be observed that the blown film of the HDPE/EVA19/C15A nanocomposite had an increase of 75% in the water vapor permeability rate compared with the pure HDPE blown film, while the blown film of the HDPE/EVA28/C30B nanocomposite had an increase of 200%. As pointed out in our earlier work,[1] the water molecules, being polar ones, will form water clusters and will diffuse more easily thru polar polymeric matrixes; because HDPE is a nonpolar polymer, the water vapor permeability rate through it will be low. However, when the EVA and nanoclay are added to the HDPE, an increase in polarity and in the amount of defects due to the formation of EVA/nanoclay discrete particles will occur and the WVPR will increase. Thus, probably the observed increase in WVPR in the blown films of nanocomposites was the result of the main transport controlling mechanism of the water clusters being thru the EVA/nanoclay particles. The WVPR was higher in the HDPE/EVA28/C30B blown film than in the HDPE/EVA19/C15A film because the latter one had a lower polarity than the first one, due to the lowest amount of VA groups in the EVA19 and to the nonpolarity of the C15A surfactant.

The oxygen permeability rates of the HDPE/EVA19/C15A and of the HDPE/EVA28/C30B blown films were 63 and 54% higher than of the pure HDPE blown film, respectively. The transport of oxygen (a nonpolar molecule) thru the pure HDPE will be high; however, the addition of the EVA and nanoclay to the HDPE will increase the polarity of the nanocomposite and, thus, a reduction in OPR is expected. In the absence of oxygen clusters, the volume of the oxygen molecule will be smaller than the water clusters and therefore the main transport controlling mechanism would be thru the EVA/nanoclay-HDPE interfaces and EVA amorphous phase; because these interfaces were highly defective, the OPR increased.

CONCLUSIONS

The twin screw mixing of HDPE and two different nanoclays (C15A and C30B) using two different EVA's (EVA19 and EVA28) as compatibilizer agents produced an intercalated structure in the HDPE/EVA19/C15A nanocomposite while in the HDPE/EVA28/C30B nanocomposite surfactant loss occurred. In both cases, however, the clay was inside the EVA phase and at the interface HDPE/EVA, forming a two-phase morphology (HDPE matrix and EVA/nanoclay discrete particles). Blown films of both nanocomposites were successfully obtained; the EVA/clay discrete particles were found to be highly oriented along the machine direction. A decrease of the average roughness of the blown films, compared with the pure HDPE film was also observed. The tensile mechanical properties along TD of all the samples was higher than along MD and all the

TABLE VI
Permeability Rates and Permeability Coefficients of the Blown Films

Blown Film	WVPR ($gH_2O/m^2.day)/\mu m$[a]	WVPC ($gH_2O.\mu m$)/(m^2.day.mmHg)	OPR [mL(CNTP)/(m^2.day)]/μm[a]	OPC [mL(CNTP).μm/(m^2.day.atm)]
HDPE	0.004 ± 0.001	5.8	1.1 ± 0.1	76.8
HDPE/EVA19/C15A	0.007 ± 0.001	8.9	1.8 ± 0.2	97.1
HDPE/EVA28/C30B	0.012 ± 0.002	13.4	1.7 ± 0.1	91.7

[a] Normalized to the film thickness.

mechanical properties along TD of the HDPE/EVA19/C15A blown film were higher than of the pure HDPE blown film. This behavior was credited to the preserved orientation from the spiral die, which oriented the HDPE lamellas along TD and to the stronger interactions between the HDPE and the EVA19 and C15A clay. The long period of the HDPE lamellas, however, was not affected by the addition of the EVA and nanoclay. Due to the formation of the two-phase morphology, the water vapor and oxygen permeability rates through the blown films of nanocomposites were higher than thru the pure HDPE blown film.

The authors thank the Brazilian Synchrotron Light Laboratory (under proposal D11A-SAXS1-3448) for the SAXS measurements, Braskem S.A. for the materials donation, Quattor Petroquímica for the use of the rheometer, Max-Planck Institute for Polymer Research and Deutscher Akademischer Auslandsdienst for the cryoultramicrotome donation and M. M. Favaro and C. A. G. Beatrice for the help in the SAXS discussions.

References

1. Lotti, C.; Isaac, C. S.; Branciforti, M. C.; Alves, R. M. V.; Liberman, S.; Bretas, R. E. S. Eur Polym J 2008, 44, 1346.
2. Shah, R. K.; Krishnaswamy, R. K.; Takahashi, S.; Paul, D. R. Polymer 2006, 47, 6187.
3. Osman, M. A.; Rupp, J. E. P.; Suter, U. W. J Mater Chem 2005, 15, 1298.
4. Alexandre, M.; Dubois, P. Mater Sci Eng 2000, 28, 1.
5. Tjong, S. C. Mater Sci Eng 2006, 53, 73.
6. Fornes, T. D.; Yoon, P. J.; Keskkula, H.; Paul, D. R. Polymer 2001, 42, 9929.
7. Beatrice, C. A. G.; Branciforti, M. C.; Bretas, R. E. S. Presented at the Polymer Processing Society 24th Annual Meeting, CD-ROM; Salerno, 2008.
8. Zhong, Y.; De Kee, D. Polym Eng Sci 2005, 45, 469.
9. Durmus, A.; Woo, M.; Kasgoz, A.; Macosko, C. W.; Tsapatsis, M. Eur Polym J 2007, 43, 3737.
10. Xu, Y.; Fang, Z.; Tong, L. J Appl Polym Sci 2007, 103, 3261.
11. Kawasumi, M.; Hasegawa, N.; Kato, M.; Usuki, A.; Okada, A. Macromolecules 1997, 30, 6333.
12. Peeterbroeck, S.; Alexandre, M.; Jérôme, R.; Dubois, P. Polym Degrad Stab 2005, 90, 288.
13. Chaudhary, D. S.; Prasad, R.; Gupta, R. K.; Bhattacharya, S. N. Thermochim Acta 2005, 433, 187.
14. Lee, H. M.; Park, B. J.; Choi, H. J.; Gupta, R. K.; Bhattacharya, S. N. J Macromol Sci Phys 2007, 46, 261.
15. Gianelli, W.; Camino, G.; Dintcheva, N. T.; Lo Verso, S.; La Mantia, F. P. Macromol Mat Eng 2004, 289, 238.
16. Lee, K. M.; Han, C. D. Macromolecules 2003, 36, 7165.
17. Zanetti, M.; Costa, L. Polymer 2004, 45, 4367.
18. Yang, H.; Song, Y.; Xu, B.; Zheng, Q. Chem Res Chin Univ 2006, 22, 383.
19. Gupta, R. K.; Prasad, R.; Chaudhary, D. S.; Kamal, M. R.; Bhattacharya, S. N. J Polym Eng 2006, 26, 805.
20. Min, K. D.; Kim, M. Y.; Choi, K.; Lee, J. H.; Lee, S. Polym Bull 2006, 57, 101.
21. Golebiewski, J.; Rozanski, A.; Dzwonkowski, J.; Galeski, A. Eur Polym J 2008, 44, 270.
22. Homepage of Southern Clay Products. Available at www.nanoclay.com,accessed in Aug 2008.
23. Trent, J. S.; Schunbum, J. I.; Couchman, P. R. Macromolecules 1983, 16, 589.
24. Martins, C. G.; Larocca, N. M.; Paul, D. R.; Pessan, L. A. Polymer 2009, 50, 1743.
25. Prasad, A.; Shroff, R.; Rane, S.; Beaucage, G. Polymer 2001, 42, 3103.
26. Xie, W.; Gao, Z.; Pan, W.; Hunter, D.; Singh, A.; Vaia, R. Chem Mater 2001, 13, 2979.
27. Marini, J.; Branciforti, M. C.; Lotti, C. Polym Adv Technol 2009; published online (doi: 10.1002/pat.1444).
28. Sukhadia, A. M.; Rohlfing, D. C.; Johnson, M. B.; Wilkes, G. L. J Appl Polym Sci 2002, 85, 2396.
29. Guerrini, L. M.; Paulin Filho, P. I.; Bretas, R. E. S.; Bernardi, A. Polímeros: Ciência e Tecnologia 2004, 14, 38.
30. Basso, G. M.; Paulin Filho, P. I.; Bretas, R. E. S.; Bernardi, A. Polímeros: Ciência e Tecnologia 2006, 16, 149.
31. Johnson, M. B.; Wilkes, G. L.; Shukhadia, A. M.; Rohlfing, D. C. J Appl Polym Sci 2000, 77, 2845.
32. Khonakdar, H. A.; Jafari, S. H.; Yavari, A.; Asadinezhad, A.; Wagenknecht, U. Polym Bull 2005, 54, 75.
33. Khonakdar, H. A.; Wagenknecht, U.; Jafari, S. H.; Hassler, R.; Eslami, H. Adv Polym Technol 2004, 23, 307.
34. Jordan, J.; Jacob, L. I.; Tannenbaum, R.; Sharaf, M. A.; Jasiuk, I. Mater Sci Eng A 2005, 393, 1.
35. Shi, X. M.; Zhang, J.; Jin, J.; Chen, S. J. Express Polym Lett 2008, 2, 623.
36. Koros, W. J.; Hellums, M. W. In Encyclopedia of Polymer Science and Engineering, supplement volume; Mark, H. F.; Bikales, N.; Overberger, C. G.; Menges, G.; Kroschwitz, J. I., Eds.; John Wiley and Sons: New York, 1989.